Positronium in xenon: The path-integral approach

Terrence Reese and Bruce N. Miller
Department of Physics, Texas Christian University, Fort Worth, Texas 76129
(Received 17 August 1992; revised manuscript received 7 December 1992)

The ability of a single positronium atom to form a semimacroscopic bubble in helium is a remarkable manifestation of quantum mechanics. Experimental evidence for bubble formation is provided by a dramatic decrease in the decay rate of the triplet state when the ambient conditions favor its formation. The phenomenon is observed near the critical point of helium and is well explained by a mean-field theory in which the positronium atom occupies the ground state of a local potential well induced by its influence on the average local density. Because of the active role played by the positronium atom in producing this localized state, the process is referred to as self-trapping. Similar experiments on other noble gases also show evidence for self-trapping near the liquid-vapor critical point, but the transition from extended to localized behavior is gradual. Mean-field theories, which ignore fluctuations, are not successful at these higher temperatures, suggesting that statistical fluctuations strongly influence the distribution over states of the light atom. This paper presents a theoretical investigation of the localization of positronium in a dense noble gas which employs the path integral to represent the translational degrees of freedom of the light atom. It demonstrates that a theoretical model which properly accounts for fluctuations is able to predict the main features of the experimental measurements.

PACS number(s): 61.20.−p, 36.10.Dr

I. INTRODUCTION

Experimental measurements of density-dependent properties of an excess light particle (electron, positron, or positronium atom) thermalized in a fluid exhibit a high degree of nonlinearity. Among these properties are electron mobility [1] and positron and positronium annihilation rates [2,3]. The accepted explanation for the nonlinearity is that the light particle (LP) creates a semimacroscopic region of altered fluid density in which it becomes localized. This process is referred to as self-trapping because of the active role played by the LP [4]. The alteration in local fluid density caused by the localization results in large changes in LP properties over small intervals of the average density of the host fluid.

Early attempts to explain self-trapping used macroscopic mean-field theory approximations, referred to here as density-functional theory (DFT). In DFT a free-energy functional is constructed that depends on the LP wave function and the local fluid density. Minimizing the free-energy functional with respect to the LP wave function and the local density results in a pair of coupled equations that self-consistently relate the LP wave function to the local fluid density. One of these is the time-independent Schrödinger equation that describes the effect of the fluid density on the LP wave function while the second determines the influence of the LP upon the local fluid density. In an earlier paper [5] it was proved that most DFT models can be derived from an appropriate density functional but that they differ in their treatment of nonlocal correlations. It is also proved that, for the simplest variant of DFT, when the thermodynamic quantities are scaled with respect to their values at the liquid-vapor critical point, the coupled equations may be expressed in a universal form and that all the system specific quantities are invested in a single dimensionless universal parameter.

DFT was successfully used to explain the decay of positrons in helium at low temperatures [6]. However, DFT is a mean-field theory and thus does not account for density fluctuations. DFT models indicate that there is a minimum threshold density below which trapping does not occur and a maximum density at which the localized state abruptly collapses. This is contrary to experiments which show a smooth transition to the trapped state instead of an easily identifiable beginning and end. While DFT models qualitatively resemble experimental measurements they tend to overemphasize localized states near the critical point, which results in plots of the decay rate versus average fluid density with incorrect shape. In a second paper [7], the authors discovered that including the possibility of transitions between the trapped and free states resulted in improvements to the decay rate calculations. Because DFT is not a microscopic model, it does not allow for the accurate determination of the correlation functions.

DFT has been surpassed lately by models directly invoking the adiabatic approximation. This is a microscopic model which most DFT's attempt to emulate in which the translational degrees of freedom of the fluid molecules are treated via classical mechanics. Miller and Fan [8] have proved that most DFT's are related to the adiabatic model through the Jensen inequality. The calculation of equilibrium quantities based on this model is achieved by using the classical isomorphism which relates the path-integral formulation of the partition function of the quantum LP to that of a closed polymer containing P fictitious particles. Computational Monte Carlo algorithms devised for classical systems may then be used to compute quantum mechanical averages for the LP-fluid

system. This method is referred to as the path-integral Monte Carlo (PIMC) technique.

The direct use of the adiabatic approximation has a major advantage over DFT. Because it is a microscopic model, it automatically includes density fluctuations and thus allows the calculation of correlation functions that may be used to determine the effects of self-trapping upon the microscopic structure of the system. While DFT has had reasonable success in modeling positron annihilation above the critical temperature, it has run into severe difficulties in predicting the decay rate of positronium. In order to determine whether the problems are connected with the essential properties of the adiabatic model rather than the method of approximation, a simulation of orthopositronium in xenon was carried out at two temperatures for which recent experimental data are available. In the simulations, the interaction between the positronium atom and the xenon atoms was represented by a hard-sphere potential and the interatomic forces were governed by the Lennard-Jones potential. Several distribution functions for the Ps-Xe system were calculated as well as the pickoff decay rate of Ps in xenon at each temperature for four values of the density to determine the density dependence of the annihilation rate. The decay rate calculations were carried out using two approximations for the xenon atom electron distribution. The first assumed that the xenon atoms had no internal structure while the second assumes that the electron distribution is rigid and may be approximated by an unperturbed Hartree-Fock potential.

We will demonstrate that a modified Monte Carlo algorithm known as staging, in conjunction with image approximation for the hard-sphere potential, results in a proper exploration of the configuration space and convergence of the theoretical results. The distribution functions obtained from this simulation show that the Ps atom becomes localized in a low-density cavity from which xenon atoms are expelled. The theoretical results indicate that the formation of the low-density cavity becomes more likely as the critical point is approached. In common with the experimental measurements, plots of the decay rate versus average density on isotherms show a smooth transition from extended to localized behavior of the LP.

The paper is divided into five sections. Section II contains a basic description of the self-trapped system in general and the importance of the decay rate of positronium as a signature of trapping. The principles and methods of the PIMC technique are outlined in Sec. III, which also contains a discussion of the distribution functions used to analyze the LP-fluid molecule system and the approximations used to compute the decay rate of Ps. The results obtained using the PIMC technique to model Ps in xenon are discussed in Sec. IV, and conclusions are given in Sec. V.

II. ENVIRONMENT

When a positron is injected into a fluid, it can either annihilate with an electron provided by a fluid molecule or it can combine with a free electron to form a positronium atom Ps. This atom shares many of its characteristics with hydrogen and has two forms: parapositronium (singlet spin state), which decays via a 2γ process with a vacuum lifetime of 1.23×10^{-10} sec, and orthopositronium (triplet spin), which requires a 3γ decay process and has the much longer lifetime of 1.45×10^{-7} sec. Due to the difference in vacuum lifetimes, after approximately 10^{-9} sec the probability of finding a surviving atom in the singlet state is small and only the triplet may be observed. Because of its long natural lifetime, the chief mode of decay of the triplet is pickoff annihilation, whereby the positron decays with an electron from the valence shell of one of the fluid molecules. In the remainder of the paper references to PS should be inferred to mean orthopositronium.

Because of its small mass, a Ps atom in a dense fluid near its liquid-vapor critical point has a deBroglie wavelength much greater than the mean separation between the molecules of the fluid. This allows the Ps atom to interact with many fluid molecules at the same time. The interaction between the Ps atom and the fluid molecules is repulsive over short distances because of the fermionic repulsion between the electron of the Ps atom and those of the fluid molecules. The combination of long deBroglie wavelength and short-range repulsion suggests that the Ps atom will attempt to create a region of low density around itself. The Ps atom may become localized in this volume. For intervals of temperature and average density where the magnitude of the decrease in free energy caused by the formation of this region of low density is greater than the increase in free energy due to the pressure-volume work required to create it, the self-trapped state will become stable [4].

The major change in the Ps-fluid system caused by the formation of the self-trapped state is the large decrease in the number of fluid molecules near the Ps atom. In attempting to detect the self-trapped state the most

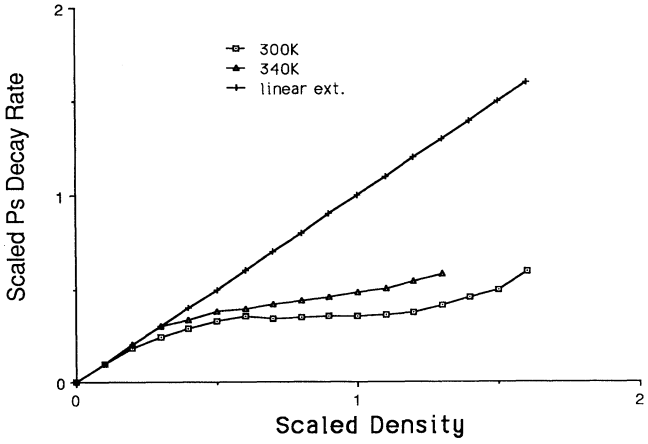

FIG. 1. Plot of the decay rate of *o*-Ps vs scaled density in xenon at 300 and 340 K. The density has been scaled with respect to the critical density. The vacuum decay rate of *o*-Ps has been subtracted from the data. The decay rate has also been scaled so that the slope of the linear extrapolation at low density is one.

straightforward course is to make measurements of quantities that are dependent on the local fluid density. The decay rate is an obvious choice because the annihilation rate of the positron is dependent upon the density of electrons in its vicinity. Figure 1 is a plot of the decay rate of Ps versus average density on two isotherms in xenon [9]. The plot passes through the origin because the vacuum decay rate of *o*-Ps has been subtracted from the data. The straight line is a linear extrapolation of the low-density behavior and is expected if the Ps atom encounters occur independently. It is apparent that the decay rate on each isotherm fails to keep up with the linear extrapolation. This deviation becomes more pronounced as the critical temperature is approached. In general, experimental isotherms of this type can be split into three regions: (i) the transition region, where an isotherm just begins to diverge from the linear extrapolation—it continues until the curve starts to flatten out and form a plateau, (ii) a region consisting of the plateau and part of the upswing of the curve that follows— in this region self-trapping predominates, (iii) a region where the isotherm rejoins the linear extrapolation and the self-trapped state collapses completely. For the xenon data displayed in Fig. 1, experimental measurements were not carried out at sufficiently high densities to observe the final upswing. However, it is readily observed in experiments on other gases [10,11].

III. PIMC

A. Discretized path-integral formulation

Since the late 1950s DFT's have dominated attempts to describe the LP-fluid molecule system. However, in the past decade, a new method for calculating equilibrium, properties of quantum-mechanical systems has become popular [12–14]. It uses the isomorphism between the discretized path-integral representation of a quantum particle [15] and the classical statistics of a ring polymer to compute quantum averages over the canonical ensemble by means of typical Monte Carlo algorithms. This method, referred to as path-integral Monte Carlo, replaces the average potential experienced by the LP in DFT models with a microscopic description of the LP-fluid molecule system. Thus the PIMC method automatically includes density fluctuations.

In contrast with the LP, in the temperature range of interest the thermal wavelength of the fluid atoms is less than 1 Å, so that their translational degrees of freedom may be treated classically. The combination of a quantum LP and a classical fluid is referred to as the adiabatic model [16]. The canonical partition function for the LP-fluid system in the ring polymer isomorphism is

$$Q=(1/\Lambda_{\rm th}^{3N}N!)\int d\underline{\mathbf{R}}\int d\underline{\mathbf{r}}\prod_{P-1\geq j\geq 0}[(m/2\pi\epsilon\hbar^2)^{3/2}\exp[-(m|\mathbf{r}_j-\mathbf{r}'_{j+1}|^2/2\epsilon\hbar^2)]\rho(\mathbf{r}_j,\mathbf{r}_{j+1},\epsilon)]\exp[-\beta U]\ , \tag{1}$$

where $\mathbf{r}_P=\mathbf{r}_0$ and $\int d\underline{\mathbf{R}}=\int d\mathbf{R}_1\cdots\int d\mathbf{R}_N$, etc. In (1), $\Lambda_{\rm th}$ is the thermal wavelength of an atom, $\underline{\mathbf{R}}$ denotes the complete set of N atomic positions $\{\mathbf{R}_j\}$, $\underline{\mathbf{r}}$ denotes the set of P positions defining the ring polymer $\{\mathbf{r}_j\}$, and $U(\underline{\mathbf{R}})$ is the total interatomic potential energy. The LP-atom interaction is accounted for by $\rho(\mathbf{r},\mathbf{r}';\epsilon)=\exp\{-\epsilon[W(\mathbf{r})+W(\mathbf{r}')]/2\}$, where $\epsilon=\beta/P$ and, as usual, $\beta=1/kT$. Finally, we assume that both the interatomic and LP-atom interactions can be effectively represented by the spherically symmetric, pairwise additive potentials $u(R)$ and $w(r)$, respectively,

$$W(\mathbf{r})=\sum_{N\geq i\geq 1}w(|\mathbf{r}-\mathbf{R}_i|)\ ,$$

$$U(\underline{\mathbf{R}})=\sum_{N\geq i>j\geq 1}u(|\mathbf{R}_i-\mathbf{R}_j|)\ . \tag{2}$$

The discretized path-integral representation of the LP has the same form as the partition function for a closed polymer chain containing P atoms. This equivalence is referred to as the classical isomorphism [16]. The quantum spread of the LP is manifested in the finite width of the distribution of classical polymer particles. Each polymer atom has a harmonic interaction with its nearest neighbors and represents the quantum particle in a different state. Each term of the transition matrix represents the probability amplitude for the quantum particle to propagate from one intermediate state to another. In the case that $P\rightarrow\infty$, the continuum limit, the density matrix may be described by the normal path integral [15].

The polymer isomorphism allows the use of classical Monte Carlo methods to compute quantum-mechanical equilibrium averages [17]. For small systems with smoothly changing potentials, accurate results can be obtained with only a limited number of polymer particles ($P\approx 10$) [18]. This property was exploited to study the structure of water in which a fluid of 125 water molecules, each with a $P=3$ discretization of the molecular orientation, was employed [19]. The Monte Carlo technique was also successfully exploited in a study of the structure of an excess electron in molten KCl [20]. Unfortunately, for systems that require rapidly changing potentials, the standard Monte Carlo (SMC) method is unsuitable.

B. Staging

As a general rule, accurate results can only be obtained from the PIMC method if the "length" of the chain between polymer atoms $[\epsilon\hbar^2/m]^{1/2}$, is small compared to the length characterizing rapid changes in the interaction potential. Thus, for rapidly changing potentials, P may become very large. For example in their study of an excess electron in xenon and helium, Coker, Berne, and Thirumalai [21] required approximately 1200 polymer particles to simulate an electron. The large number of polymer particles required for systems with rapidly

changing potentials leads to several problems that make the use of the traditional SMC method unreliable for simulating the LP-fluid molecule system.

The potential energy in the harmonic bond between the polymer particles is proportional to P. Because of the strong potential between polymer particles in systems with large P it is very likely that a new acceptable position for a particle will be very close to its previous position if only a single polymer particle is moved at one time. Sequential configurations generated in this manner will be highly correlated. Because of the high correlation between new acceptable configurations and old ones, a long time will be required before movements of single polymer particles result in large scale changes in overall polymer structure. Unfortunately, this means it will require a large number of passes for the system to reach equilibrium. A further complication is introduced if the LP-atom potential is repulsive. This results in a small probability of acceptance of a given Monte Carlo move. The combination of high correlation between polymer configurations and long equilibration times results in a slow sampling of the configuration space.

These problems have been understood for years and many researchers have devised a number of alternative Monte Carlo methods to address them [18,21–24]. Generally these methods employ some means of directly sampling the distribution of free harmonic bond lengths for the chain. Bartholomew, Hall, and Berne [22] use the normal modes of the chain as random variables. This method is known to be equivalent to the Fourier series path-integral technique [25] which has been shown to be incapable of overcoming the slow sampling of the configuration space inherent in the SMC technique [25]. Worrell and Miller [26] have used the method pioneered by Ceperley and Pollock [24] to compute the decay rate of positrons in xenon.

Sprik, Klein, and Chandler [18] have introduced a method known as staging in which a small number of primary particles are used to create large-scale fluctuations in the polymer structure. A large number of configurations of secondary particles are then created between each of the primary particles and their average probability is used to accurately determine the proper statistical weight of the given primary particle configuration. In this method an entirely new primary chain is laid down with every pass, thus bypassing the problem caused by the slow evolution of the large scale polymer structure within the SMC technique. The small number of primary particles decreases the likelihood of rejection of the new polymer configuration because of unfavorable LP-fluid molecule interaction potentials, which is a major problem for Monte Carlo methods that directly sample the free harmonic bond lengths.

C. Image potential

Because of the dominance of the short-range repulsion in Ps-fluid molecule interactions, the hard-sphere potential was considered the best candidate to represent the polymer particle-fluid molecule interaction potential. The effect of the hard-sphere potential vanishes outside the boundary of the P polymer particles. Its effect upon the density matrix is given by

$$\rho(\mathbf{r},\mathbf{r}',\mathbf{R}_i;\epsilon)=\begin{cases}1\ , & |\mathbf{r}-\mathbf{R}_i|\geq d\\ 0\ , & |\mathbf{r}-\mathbf{R}_i|<d\ ,\end{cases} \tag{3}$$

where $\mathbf{R}_i$ is the vector representing the position of fluid molecule i and d is the hard sphere diameter, the closest distance of approach between the centers of a polymer particle and a fluid molecule. Equation (3) is referred to as the primitive approximation [18].

In the examples given at the end of Sec. III A the traditional SMC was able to give accurate results for systems that require only a limited number of polymer particles (systems with smooth potentials). However, it fails badly for systems with steep potentials because a large number of polymer particles are required to accurately simulate the LP-fluid molecule interaction. These problems are compounded by the use of the hard-sphere potential, for which $\rho(\mathbf{r},\mathbf{r}';\epsilon)$ is a step function. In other words, an infinite number of polymer particles is required to satisfy the criterion that $\hbar\sqrt{\beta/mP}$ is less than the distance over which the potential changes rapidly.

Barker proposed an approximation to the normalized density matrix, based upon the image method, which forces the correct boundary conditions at the hard-core surfaces [27]. This results in a decrease in the number of polymer particles required for convergence. In these calculations, we will use the image approximation devised by Whitlock and Kalos [28]

$$\rho(\mathbf{r},\mathbf{r}',\mathbf{R}_j;\epsilon)=\begin{cases}1-\exp[-2PF(\mathbf{r},\mathbf{r}',\mathbf{R}_j)]\ , & |\mathbf{r}-\mathbf{R}_j|\ ,\ |\mathbf{r}'-\mathbf{R}_j|>d\\ 0\ \text{ otherwise}\ ,\end{cases} \tag{4}$$

where

$$F(\mathbf{r},\mathbf{r}',\mathbf{R}_j)=(|\mathbf{r}-\mathbf{R}_j|^2-d^2)(|\mathbf{r}'-\mathbf{R}_j|^2-d^2)/(\Lambda_{\mathrm{LP}}d)^2\ , \tag{5}$$

Λ_{LP} is the LP thermal wavelength, and $|\mathbf{r}-\mathbf{R}_j|$ and $|\mathbf{r}'-\mathbf{R}_j|$ are the respective distances between the fluid molecule at $\mathbf{R}_j$ and the polymer particles at $\mathbf{r}$ and $\mathbf{r}'$. Calculations by Liu and Broughton [29] indicate that this approximation converges more rapidly than the approximation devised by Barker. The interaction between the fluid molecules is represented by the Lennard-Jones 6-12 potential.

D. Important properties

1. Structural quantities

The properties that can be determined from an equilibrium Monte Carlo study of the LP-fluid molecule system can be divided into two types, structural and thermodynamic. Structural quantities detail information con-

cerning the local polymer-fluid and fluid-fluid structure on a microscopic level. For example, the polymer-fluid radial distribution function

$$g_{fp}(r)=\rho^{-1}\left\langle \sum_{N\geq i\geq 1} P^{-1} \sum_{P-1\geq k\geq 0} \delta(\mathbf{R}_i-\mathbf{r}_k-\mathbf{r})\right\rangle \quad (6)$$

gives information concerning the local fluid environment around the polymer particles. Information concerning the average density of the fluid about the geometric center of the polymer is provided by the distribution function

$$g_{fc}(\mathbf{r})=\rho^{-1}\left\langle \sum_{N\geq i\geq 1} \delta(\mathbf{R}_i-\mathbf{r}_{\text{c.m.}}-\mathbf{r})\right\rangle . \quad (7)$$

It can be used to determine whether localization occurs at a certain density and temperature, and the size of the well formed by the localized polymer. Most physical properties of the fluid can be determined from the intermolecular radial distribution function

$$g_{ff}(R)=\rho^{-1}\left\langle \sum_{N\geq i>j\geq 1} \delta(\mathbf{R}_i-\mathbf{R}_j-\mathbf{R})\right\rangle . \quad (8)$$

Information concerning the behavior of the polymer may be determined from the mean-square displacement (MSD) between two polymer particles on the chain separated by an imaginary time interval of $t-t'$ $[0\leq(t-t')\leq\beta\hbar]$, $R^2(t-t')\equiv\langle|\mathbf{r}(t)-\mathbf{r}'(t')|^2\rangle$. For a free particle this function is given by [16]

$$R^2(t-t')=3\Lambda_{\text{LOP}}^2(t-t')[\beta\hbar-(t-t')]/(\beta\hbar)^2 . \quad (9)$$

For an extended LP, a plot of $R(t-t')$ vs $t-t'$ has the shape of an inverted parabola with a strong maximum at $\beta\hbar/2$. This should be compared with the case of a highly localized polymer configuration, where the value of the MSD is practically independent of the imaginary time difference except near the end points 0 and $\beta\hbar$.

2. Decay rate

The pickoff decay rate of PS is proportional to the overlap between the positron of the Ps atom and the effective density of fluid electrons of opposite spin available for annihilation. The electron charge distribution around a fluid nucleus at $\mathbf{R}'$ is defined as $f(|\mathbf{R}'-\mathbf{r}|)$, where r is the position at which the charge distribution is to be determined. The quantum-mechanical decay rate operator for a positron at $\mathbf{r}_+$ is then given by

$$\hat{\lambda}=\sum_{N\geq j\geq 1} f(|\mathbf{R}_j-\mathbf{r}_+|) \quad (10)$$

(the position of the Ps electron is given by $\mathbf{r}_-$) [8]. If we express (10) in terms of $\mathbf{r}_{\text{c.m.}}$ $(\equiv(\mathbf{r}_++\mathbf{r}_-)/2]$, the center of mass of the Ps atom, and ω $(\equiv\mathbf{r}_+-\mathbf{r}_-)$, the vector distance between the positron and the electron, we arrive at

$$\langle\psi|\hat{\lambda}|\psi\rangle=\int\int \sum_{N\geq j\geq 1} f(|\mathbf{R}_j-\mathbf{r}_{\text{c.m.}}-\boldsymbol{\omega}/2|)|\varphi_0(\omega)|^2 \times|\psi_0(\mathbf{r}_{\text{c.m.}})|^2 d\boldsymbol{\omega}\, d\mathbf{r}_{\text{c.m.}} , \quad (11)$$

where, in (11), we have assumed that the Ps wave function separates into the overall translational factor $\psi_0(\mathbf{r}_{\text{c.m.}})$ and the relative factor $\varphi_0(\omega)$.

In the approximation employed here, both the positronium atom and the fluid molecules are treated as composite particles. The path integral represents the translational coordinates of the positronium atom. Thus, in the discrete version,

$$|\psi_0(\mathbf{r}_{\text{c.m.}})|^2=\frac{1}{P}\sum_{i=0}^{P-1}\delta(\mathbf{r}_i-\mathbf{r}_{\text{c.m.}}) ,$$

where $\mathbf{r}_i$ is the position of polymer particle i. If we assume that the internal state of Ps is unaffected by the presence of the fluid molecules, then $\varphi_0(\omega)$ may simply be approximated by the ground-state wave function, so that

$$|\varphi_0(\omega)|^2=\exp[-\omega/a_0]/8\pi a_0^3$$

where, as usual, a_0 is the Bohr radius. Addressing these points in (11) yields

$$\langle\psi|\hat{\lambda}|\psi\rangle=(1/8\pi P a_0^3) \times\sum_{P-1\geq i\geq 0}\sum_{N\geq j\geq 1}\int d\omega\exp[-\omega/a_0] \times f(|\mathbf{R}_j-\mathbf{r}_i-\boldsymbol{\omega}/2|) . \quad (12)$$

The mean value of the decay rate in the adiabatic model is given by [8]

$$\lambda\equiv\langle\hat{\lambda}\rangle=(1/Z)\int d\mathbf{R}\int d\mathbf{r}\langle\psi|\hat{\lambda}|\psi\rangle D(\underline{\mathbf{r}})\exp[-\beta U(\underline{\mathbf{R}})] , \quad (13)$$

where

$$D(\underline{\mathbf{r}})\equiv\prod_{j=0}^{P-1}(m/2\pi\epsilon\hbar^2)^{3/2} \times\exp[-(m|\mathbf{r}_j-\mathbf{r}'_{j+1}|^2/2\epsilon\hbar^2)] \times\rho(\mathbf{r}_j,\mathbf{r}_{j+1},\epsilon) ,$$
$$Z=\int d\underline{\mathbf{R}}\int d\underline{\mathbf{r}}\, D\exp[-\beta U] . \quad (14)$$

From (13) it is clear that the decay rate operator consists of a pairwise sum, where each polymer particle-atom pair contributes

$$\lambda'(|\mathbf{R}_j-\mathbf{r}_i|) ,$$
$$\lambda'(|\mathbf{R}_j-\mathbf{r}_i|)=(1/8\pi P a_0^3) \times\int d\omega\exp[-\omega/a_0]f(|\mathbf{R}_j-\mathbf{r}_i-\omega/2|) . \quad (15)$$

Thus λ is governed by g_{fp}, the polymer-fluid radial distribution function. Summing over all pairs and substituting in (13) yields, for the thermal average of $\hat{\lambda}$,

$$\lambda=(1/8\pi a_0^3)\rho\int d\mathbf{R}'\int d\boldsymbol{\omega}\exp[-\omega/a_0] \times f(|\mathbf{R}'-\boldsymbol{\omega}/2|)g_{fp}(R') , \quad (16)$$

where $\mathbf{R}'$ is the vector distance between a polymer particle and a fluid molecule $R'=|\mathbf{R}'|$ and ρ is the average fluid density. Miller and Fan have derived a similar expression for the decay rate of a *positron* in a classical fluid [8].

Equation (16) determines the mean decay rate of the Ps in the fluid. The main approximations are the separability of the positronium state vector and the form of the electron density f. In our calculations we have used two approximations for f. The first represents the electron distribution as a delta function $[f(|\mathbf{R}-\boldsymbol{\omega}/2|) = \delta(\mathbf{R}-\boldsymbol{\omega}/2)]$. If we remember that $\delta(\mathbf{R}-\boldsymbol{\omega}/2) = 8\delta(2\mathbf{R}-\omega)$ and carry out the integral over ω in (16) we obtain

$$\lambda=\rho\int d\mathbf{R}\exp[-2R/a_0]g_{fp}(R)/(\pi a_0^3)\ . \tag{17}$$

In the δ-function approximation the decay rate is merely the overlap of the molecular coordinates and the portion of the positron wave function outside the hard-sphere diameter.

The second approximation also assumes that the positron does not induce any perturbations in the fluid molecule wave function. However, rather than being concentrated at a point, the electron density is taken from the Hartree-Fock solution for the atomic orbitals. In this work the Laplacian of the Hartree-Fock potential for xenon was used to compute a table of values for the electron distribution [30]. It was determined that the unperturbed electron distribution for xenon can be adequately represented by a sum of Yukawa functions

$$f(x)=\alpha\exp[-ax]/x+\beta\exp[-bx]/x\ , \tag{18}$$

where α, β, a, and b are constants that are determined from a least-squares fit with the data table. If (18) is employed in the integral over $\boldsymbol{\omega}$ we arrive at the expression

$$\lambda=\rho\int d\mathbf{R}[AaI_3(a)+(1-A)bI_3(b)]g_{fp}(R)/(2Ra_0^3)\ ,$$

$$I_3(a)=2a\exp[-aR]/(a_0c^2) -\exp[-2R/a_0][2Ra/c+2a/(a_0c^2)]\ , \tag{19}$$

$$c=(1/a_0)^2-(a/2)^2\ ,$$

where $I_3(b)$ is simply $I_3(a)$ with b replacing a, $A=\alpha/a$, and $(1-A)=\beta/b$. In the self-consistent field (SCF) approximation the electron density is now allowed to penetrate the hard-sphere diameter, which results in a greater overlap between the electron density and the positron wave function. This should increase the likelihood of an annihilation with the positron and result in a higher value of the decay rate for the extended SCF function than for the δ-function approximation.

Figure 2(a) compares $\lambda'(r)$ for these two cases. In the first case, where the electronic charge is assumed to be concentrated at a point, the value of $\lambda'(0)$ is almost ten times the value for the extended charge distribution. However, it goes to zero near 1.8 Å, well before the extended distribution, which has a much larger effective range. From (17) it is clear that $r^2\lambda'(r)$ is the relevant quantity for the decay rate. This is plotted for each case in Fig. 2(b) where the difference in the falloff of the two functions can be seen much more readily. In the case of the δ function, $r^2\lambda'$ has approximately the shape of a Gaussian while the extended charge distribution results in a long tapering tale.

For the δ-function charge distribution the mean decay rate may also be calculated by computing the value of

$$\tilde{\lambda}[=(1/8\pi Pa_0^3)\sum_{j=1}^{N}\sum_{i=0}^{P-1}\exp[-2|\mathbf{R}_j-\mathbf{r}_i|/a_0])$$

for each pass and then computing the average. The results of this calculation and the results from the mean decay rate calculated using the radial distribution function provide a consistency check on the resolution of the distribution functions. If the results of the methods closely agree, then it is reasonably certain that an appropriate value for the minimum resolution of the histogram of the distribution functions has been chosen. The variance of the decay rate σ_λ^2, which is determined by computing $\langle\hat{\lambda}^2\rangle-\langle\hat{\lambda}\rangle^2$, characterizes the spread around the average decay rate. This is an important measure of fluctuations in the Ps environment which is not obtainable from DFT's.

E. Algorithm

An algorithm was devised to take advantage of the staging method to calculate the structural and thermodynamic properties of Ps in fluids. The algorithm is

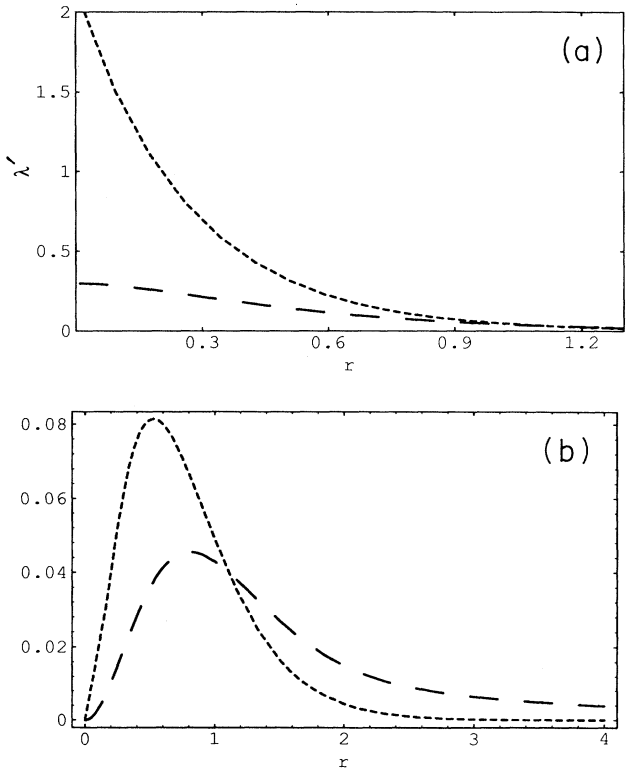

FIG. 2. (a) Plot of $\lambda'(r)$ vs r for the δ-function approximation and the Hartree-Fock approximation for the electron distribution function used to approximate the decay rate. The curve composed of long dashes corresponds to the extended SCF overlap function; the short dashes correspond to the δ-function electron charge distribution. (b) Plot or $r^2\lambda'$ vs r for the δ-function approximation and the Hartree-Fock approximation for the electron distribution function. The code is the same as in (a).

dependent upon four characteristic parameters Λ_{Ps}, the Ps thermal wavelength σ, the Lennard-Jones distance scale ρ^* ($\equiv\rho\sigma^3$), the average density of the fluid, and d, the hard-sphere diameter. The only parameter that is not already known is the value of d. It will have to be estimated or determined from comparisons between theoretical computations and experimental results. In preliminary calculations it was discovered that, at densities approaching the critical density, convergence is unlikely to occur within a reasonable number of passes. The problem arises because, at higher densities, the recreation of an entirely new primary polymer chain at each pass results in a high initial rejection rate due to the large probability of overlap between the polymer particles and fluid molecules. Thus, out of a large number of primary polymer configurations, only a few will be used to compute the properties of the Ps-fluid system. Because of this discovery, and in contrast with other implementations of staging [18], the algorithm was modified so that only a segment of primary particles is moved at one time.

The algorithm first creates an initial configuration for the system. The initial primary polymer configuration is set up in accordance with Levy's recursive scheme for directly sampling conditional Brownian motion paths [31,21]. The initial point on the primary chain is randomly selected in a cube having sides of length $3\Lambda_{Ps}$. The fluid molecules are randomly distributed within the cube with the only constraint being that the distance between the center of any fluid molecule and any polymer particle must be greater than d. The energy and the statistical weight of the initial configuration is then computed. The weight and kinetic energy of the LP is calculated by the original staging method.

The image potential is used to determine the effective polymer-fluid interaction energy for each of the secondary particles. A number of secondary particle configurations are created between each primary particle and its neighbor and the value of the statistical weight for each secondary configuration is calculated. The Metropolis algorithm is then used to calculate the value of the statistical weight for the primary configuration.

New configurations for the primary particles may now be generated by moving chain segments of length n. A new trial configuration of the segment is generated by using Levy's iterative procedure for creating an entirely new primary polymer configuration [21]. This procedure is repeated, traversing the primary polymer chain until the primary particle is reached that is n particles away from the starting particle. Thus, only the initial primary particle remains stationary. After each attempted segment move, a set of secondary configurations are grown between each of the new primary particles and used to determine the weight of the new segment configuration and whether or not it will replace the old segment configuration.

Because the starting primary particle is not moved there are $P_a - n$ attempted segment moves per pass where P_a is the number of particles in the primary chain. The completion of this process results in a different configuration for the primary polymer particles after every pass. After the new polymer configuration has been established, the traditional SMC technique is used to create a new configuration for the fluid molecules. Averaging, in which only the primary particles contribute, is carried out over the desired quantities after every pass. The computation of the partition function Q leads to the system free energy through the equation $A=(-1/\beta)\ln(Q)$, where A is the Helmholtz free energy.

Theoretically, the creation of a new polymer configuration every pass results in a high probability of large-scale fluctuations in the polymer structure. In practice, the low acceptance rate due to the high likelihood of overlap between polymer particles and fluid molecules leads to very slow convergence. The use of chain segments to create new polymer configurations results in a much lower rejection rate of trial configurations. However, the smaller the chain segment, the lower the probability that large-scale fluctuations in the polymer structure will occur. Thus it is important for the chain segment length to be large enough to allow large-scale fluctuations in the structure to occur over a reasonable amount of time without making it so large that the rejection rate becomes too high to allow for exploration of the configuration space.

The staging algorithm has an advantage over several other methods used to overcome the slow convergence of the SMC technique. Because the positions of the secondary particles depend only upon the end points, it is more amenable to vectorization. In addition, the same Gaussian random numbers can be reused to calculate the secondary configurations between different primary particles because the secondary configurations are independent. This results in some saving in time due to the continued reuse of previously calculated Gaussian random numbers.

IV. RESULTS

A. Convergence

In order to ascertain if the PIMC technique in conjunction with the image approximation is capable of simulating the Ps-fluid molecule system, calculations were made using the Lennard-Jones 6-12 parameters for xenon ($\sigma=4.0551$ Å, $\epsilon=229$ K) to model the fluid. The calculations were made at four densities: $\rho^*=0.017$, 0.088, 0.17, and 0.35 ($0.05\rho_c$, $0.25\rho_c$, $0.5\rho_c$, and ρ_c) for each of two temperatures ($T=300$ and 340 K). For reasons which will be explained in Sec. IV C below, d was selected to be 2.5 Å. In order to minimize the influence of finite-size effects, the length of the side of the cube in which the calculations take place is $3\Lambda_{Ps}$. The total number of fluid molecules was determined by this size and the average density.

If a Monte Carlo algorithm is to be considered successful it must first be demonstrated that its results are reliable. The goal of the computations described here is to obtain statistical averages which are correct in the thermodynamic limit. This requires that the number of molecules, the number of polymer sites, and the number of passes through the system be sufficiently large that the averages of interest are not significantly altered if they

are increased. This reliability of results is referred to as convergence. There are two types of convergence. The first type is convergence with respect to the number of passes. This property is used to determine whether the results approach an equilibrium value or continue to fluctuate indefinitely. To ensure that the number of system passes was sufficient in each case, the average root-mean-square displacement (RMSD) at the polymer halfway point ($\sqrt{\langle R^2(\beta\hbar/2)\rangle}$) and the average decay rate were continuously monitored. They usually converged after about 5000 passes; however, the RMSD value converged more rapidly as the density was increased. The calculations were carried out to 10 000 passes in order to ensure that the results had stabilized. In each of the calculations, the initial configurations were allowed to anneal for 1000 passes before averaging commenced.

The second kind of convergence is stabilization with respect to the algorithm's extensive quantities, such as particle number. In other words, it is important to ensure that increases in polymer number and total molecular population will not lead to changes in the computed results. Unfortunately, the radial distribution functions showed a slower convergence with particle number. Since these quantities are dependent upon the primary particles it is possible to increase their number and leave the number of secondary particles stable at 32. The largest polymer required 44 primary particles to stabilize g_{fp}. Size effects were minimized by choosing the overall system size to be at least three times the thermal wavelength of the LP.

B. Structural results

Figures 3(a) and 3(b) are plots of the RMSD for each of the four densities at $T=300$ and 340 K. The RMSD gives an indication of the number of states available to the system. In both figures $\rho^*=0.0$ is the theoretical result for a polymer that has no fluid molecules to interact with. At $\rho^*=0.017$, the RMSD is very near the value for the free polymer in both cases. As the density is increased, the number of states available to the polymer decreases until, at the critical density ($\rho^*=0.35$), the value of the RMSD for 30 out of the 44 primary particles are within 5% of the value at the midpoint ($\beta\hbar/2$), indicating that the polymer is highly compressed. Moreover, it is clear from the figure that the maximum extent of the polymer at the critical density is roughly half that of the free particle, revealing a strong tendency of the Ps to localize. In the remainder of this subsection, differences between the trapped and the extended state for the structural quantities defined in Sec. III D will be explored.

Figures 4(a) and 4(b) are plots of the two polymer-fluid distribution functions defined in Sec. III D for $\rho^*=0.017$ and 0.35 at $T=300$ K. In Fig. 4(a) there is no restriction on the polymer center (g_{fp}), while in Fig. 4(b) it is constrained to lie at the origin (g_{fc}). These plots can be used to evaluate the microscopic differences between the extended and the localized states. Figure 4(a) shows that while both distribution functions begin to increase at $r\approx 2.5$ Å, at the lower density, the increase occurs more rapidly than at the critical density. In fact, the extended state begins to level off well before 10 Å while the distribution function for the localized state continues to increase beyond 10 Å. Beyond 10 Å the distribution function at the critical density is slightly greater than one. The system size does not allow us to determine whether this is a finite-size effect or the beginning of a small oscillation resulting from the intermolecular repulsion at short distances. These results also support the expectation that fluid molecules are more easily displaced at the critical density. Figure 4(b) shows a nonvanishing value of $g_{fc}(r)$ for $\rho^*=0.017$ as $r\to 0$. This suggests that the polymer on occasion envelops fluid molecules. However, for the localized state, $g_{fc}(r)\to 0$ as $r\to 0$, indicating that the polymer has been compressed and has completely expelled fluid molecules from the vicinity of the polymer center. Experimental results indicate that trapping becomes more likely as the liquid-vapor critical point is approached. This result is also indicated in Figs. 5(a) and 5(b), which are plots of the polymer-fluid and fluid-polymer center radial distribution functions at the critical density for $T=300$ and 340 K. In each plot the value of the respective distribution function is greater for $T=340$ K than for $T=300$ K, except near the cell boundary, where both functions level off. This indicates that at

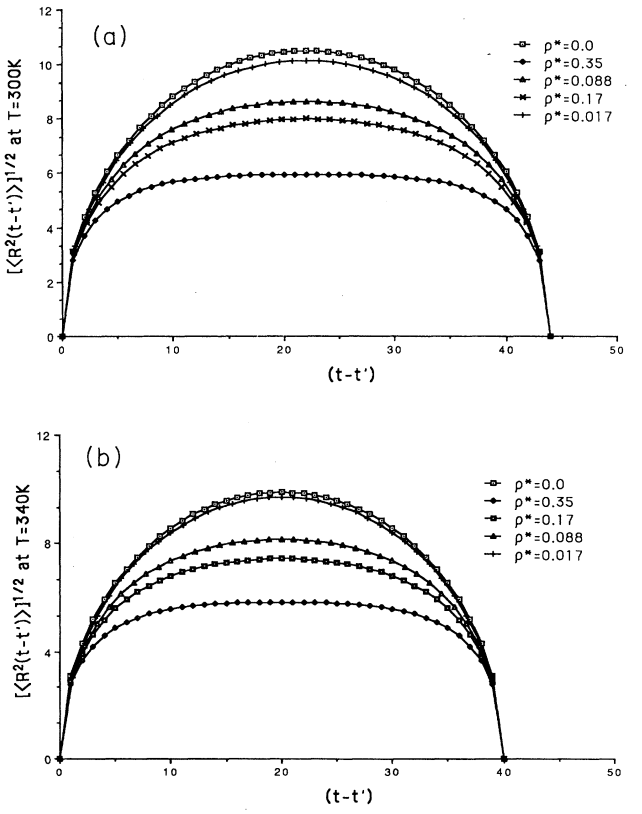

FIG. 3. (a) Plot of the RMSD vs the imaginary time interval for $\rho^*=0.0$, 0.017, 0.008, 0.17, and 0.35 at $T=300$ K. $\rho^*=0.0$ represents RMSD for a polymer particle that does not interact with any fluid molecules. Note that localization increases with density. (b) Plot of RMSD vs imaginary time for $\rho^*=0.0$, 0.017, 0.088, 0.17, and 0.35 at $T=340$ K.

$T=300$ K the fluid molecules are more easily displaced than at $T=340$ K.

In general, the polymer centered radial distribution is far more noisy than the ordinary fluid-polymer radial distribution function. This is a consequence of the information loss incurred by conditioning on the polymer center. However, at distances less than 10 Å, $g_{fc}(r)$ is much smoother for the critical density at both temperatures than for $\rho^*=0.017$ indicating that, as the LP becomes more confined, the density fluctuations in its vicinity decrease. We will have more to say about this in the next subsection.

C. Decay rate

An important goal of this project is to recreate the transition region in experimental measurements of the Ps pickoff decay rate. Theoretical computations of the pickoff decay rate based on DFT indicate a sudden turning on or off of the localized state. Below a threshold density the LP is undoubtedly extended and above a certain density, depending upon the temperature, localization collapses. However, experiments show a smooth transition from the extended to the localized state, instead of a discontinuity where localization begins and ends. The reason for this incongruity is that DFT's ignore density fluctuations which are important in most fluid phenomena. Because PIMC is a microscopic model it automatically includes the density fluctuations and thus has a better chance of recreating the transition region.

Equation (17), which can be used to calculate the Ps decay rate, requires an accurate determination of $g_{fp}(r)$. The polymer-fluid radial distribution function as calculated with our algorithm is a histogram in which the density of fluid molecules is computed with a shell of width *dr*. The value of *dr* is the resolution of the histogram: Smaller values of *dr* result in a more accurate determination of the distribution function, but require longer computation times to obtain good statistics. It is important to determine a practical value for *dr*. In Sec. III it was stated that the mean decay rate for the δ-function approximation may also be calculated by computing

$$\tilde{\lambda}=(1/8\pi Pa_0^3)\sum_{i=0}^{P-1}\sum_{j=1}^{N}\exp[-2|\mathbf{R}_j-\mathbf{r}_i|/a_0] \tag{20}$$

after each pass. The mean decay rate is the sum of the $\tilde{\lambda}$'s for each pass divided by the total number of passes. Using this method, the accuracy of the decay rate is dependent upon the number of passes, but not *dr*. The

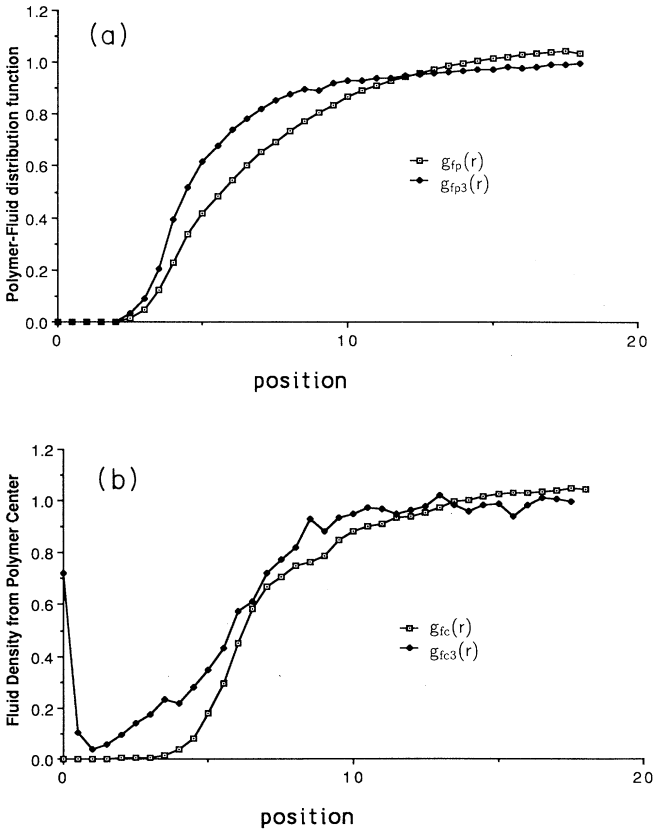

FIG. 4. (a) Plot of the polymer-fluid radial distribution function vs position for $\rho^*=0.017$ $[g_{fp3}(r)]$ and 0.35 $[g_{fp}(r)]$ at $T=300$ K. (b) Plot of the density of fluid molecules measured radially from the polymer center of mass vs position for $\rho^*=0.017$ $[g_{fc3}(r)]$ and 0.35 $[g_{fc}(r)]$ at $T=300$ K.

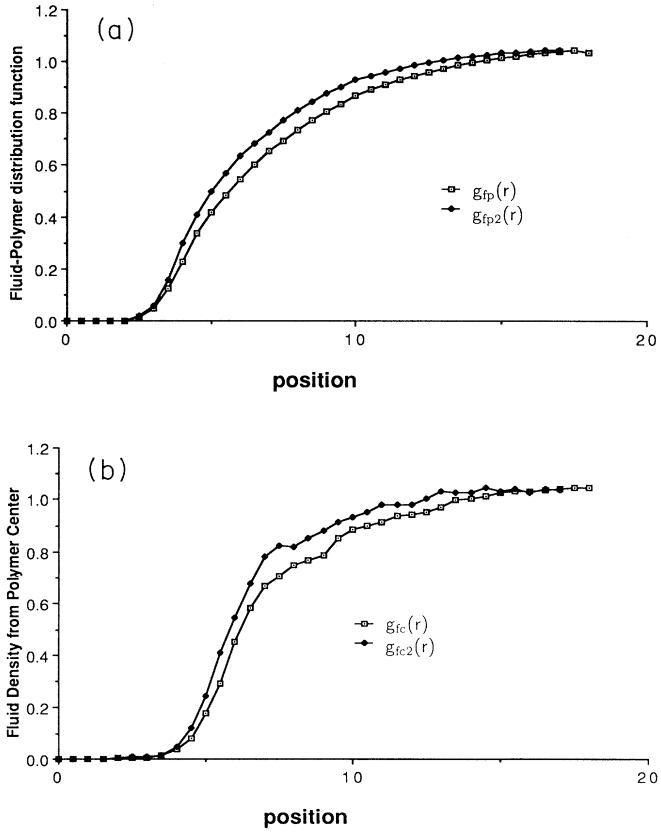

FIG. 5. (a) Plot of the polymer-fluid radial distribution function vs position for $\rho^*=0.35$ at $T=300$ K $[g_{fp}(r)]$ and 340 K $[g_{fp2}(r)]$. (b) Plot of the density of fluid molecules measured radially from the geometric center of the polymer for $\rho^*=0.35$ at $T=300$ K $[g_{fc}(r)]$ and 340 K $[g_{fc2}(r)]$.

value of the mean decay rate calculated using (20) can be used to determine a useful value of dr for $g_{fp}(r)$. In our preliminary tests it was determined that 0.1 Å provides sufficient accuracy. It is less than $\frac{1}{20}$ of any of the significant length scales in the system. Computation of the mean decay rate via (16) has the major advantage that it allows the use of different electron density functions f to be tested without having to run the entire computations over again.

The most important fluid specific value that needs to be determined for the computation of the decay rate is the hard sphere diameter d. It determines the minimum separation between a polymer particle and fluid molecule and thus determines the shape of the polymer-fluid radial distribution function. The larger the value of d, the smaller the value of $g_{fp}(r)$ at shorter distances, and the lower the probability of an overlap between the atomic electrons and the positron wave function. A possible candidate for d may be estimated if we compute the ratio R_E of the experimental value of the decay rate at a specific density to the value of the linear extrapolation at that same density, and use it to help determine an approximate value for d. The critical density is a good choice because it is known that the experimental deviation from linearity there is large, thus minimizing the influence of experimental uncertainty. If we designate λ_0 as the value of the linear extrapolation and λ_e as the value of the experimental decay rate at the critical density, then $R_E=\lambda_e/\lambda_0$. The ratio of λ_d, the decay rate computed by the algorithm at a given value of d at the critical density, to λ_0 (from the simulation) is defined as R_T. It was judged that if $R_T \approx R_E$, then an approximate value for d had been determined.

Because of the certainty that the Ps atom is extended at the density $\rho^*=0.017$, its decay rate was computed from the simulation and then used to determine the value of the linear extrapolation at the other three density values. It was assumed that the minimum value of d was $\sigma/2$ which for xenon meant that $d \geq 2.0$ Å. The resulting tests indicated that $d=2.5$ Å was a more useful (accurate) value of the hard sphere diameter than 3.0 Å. This turns out to be half the sum of the Lennard-Jones diameter and the mean e^+-e^- separation in positronium. The decay rate was calculated at $\rho^*=0.017$ for both $T=300$ and 340 K at $d=2.5$ Å. In common with the experimental observations, the decay rates are nearly the same for the two temperatures, which is an indication that 2.5 Å is an appropriate, if not precise value for d.

Figures 6(a) and 6(b) are plots of the decay rate obtained using the δ-function approximation at the four density points for $T=300$ and 340 K, respectively. The decay rate is scaled such that the value of the linear extrapolation is equal to one at the critical density. The experimental curves, similarly scaled, are also plotted for comparison. In each figure the theoretical decay rates for $\rho^*=0.088$ and 0.17 are very close to the experimental values for those densities. However, at the critical density there is a divergence between experimental and theoretical decay rates. The percentage difference between R_E and R_T is the same for both $T=300$ and 340 K. In each case the value of the computed decay rate is greater than the experimental measurements, suggesting a greater tendency for localization of Ps at the critical density than the model predicts. Table I compares the results obtained by using the δ function with the Hartree-Fock electron distribution. As can be seen there is only a 2% difference between the decay rates calculated for $\rho^*=0.17$ and 0.35 using the extended function, suggesting that, in this version of the model, there are too many electrons in the vicinity of the positron.

The variability of the environment the Ps atom experiences may be studied by examining ζ_λ, the ratio of the standard deviation σ_λ to the mean decay rate. Small values of ζ_λ suggest that the LP experiences small density fluctuations. However, a value of ζ_λ near unity indicates the presence of large local fluctuations in the density. In ascending order for each of the four density points at $T=300$ K the values of ζ_λ are 0.75, 0.5, 0.45, and 0.44. It is not surprising that the value of ζ_λ is large at small densities where density fluctuations are known to be large. It is noteworthy that ζ_λ remains significant at the higher densities. This *may* result from the increase in compressibility as the critical point is approached.

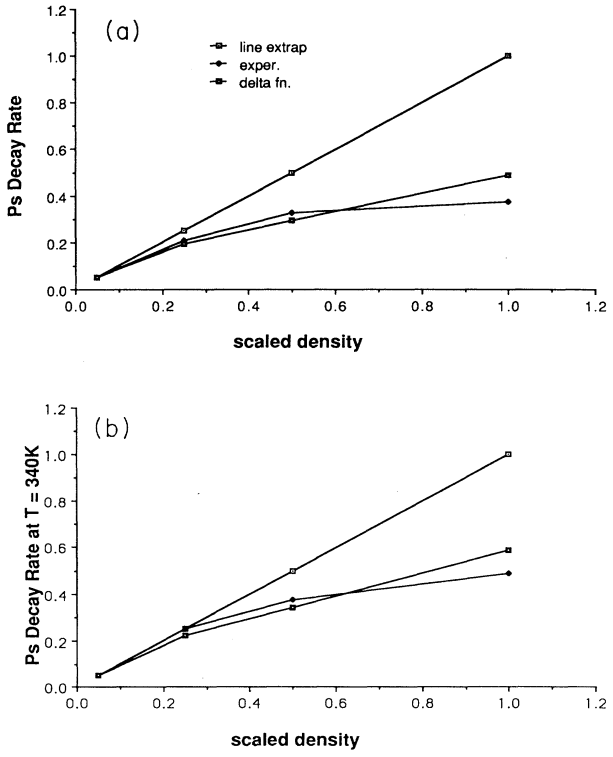

FIG. 6. (a) Plot of the experimental and theoretically calculated decay rate of Ps in xenon vs density on the isotherm $T=300$ K. The calculation was done using the δ-function approximation for the electron charge distribution. (b) Plot of the experimental and theoretically calculated decay rate of Ps in xenon vs density on the isotherm $T=340$ K. The calculation was done using the δ-function approximation for the electron charge distribution.

TABLE I. Comparison of results obtained with the δ-function Hartree-Fock electron distribution.

ρ^*	$ip \times np$	λ_E	λ_{T_1}	λ_{T_2}	ζ_V
		$T=300$ K			
0.017	36×36	1.0	1.0	1.0	0.75
0.088	40×32	83.4%	78%	87%	0.5
0.17	40×32	65.6%	59%	73.6%	0.45
0.35	44×32	37.4%	49%	71%	0.44
		$T=340$ K			
0.017	36×32	1.0	1.0	1.0	0.83
0.088	36×32	1.0	90%	94%	0.5
0.17	40×32	75%	68%	86%	0.45
0.35	40×32	49%	59%	84%	0.4

V. CONCLUSION

Early models that were used to describe the LP-fluid molecule system relied on DFT as an approximation to the adiabatic model. However, the failure of models based on DFT to accurately reproduce experimental measurements of LP properties in fluids spurred attempts to create a *microscopic* model of the LP-fluid molecule system. The classical isomorphism exploits the equivalence between the discretized path-integral representation of a quantum particle and the classical partition function of a closed polymer molecule. It thus allows the statistical methods developed for classical systems to be used in the computation of equilibrium averages for quantum-mechanical systems. Because it is a microscopic model the PIMC technique automatically includes the effect of both density and quantum fluctuations on the averages of the desired properties, which is lacking in most realizations of DFT.

A consequence of the large number of polymer particles required to approximate the rapidly changing potentials used to simulate the LP-fluid molecule interactions is that the SMC is incapable of sampling the configuration space in a reasonable amount of time. A modification of the staging algorithm overcomes this problem by building up the total chain configuration in stages. The first stage, which consists of a small number of polymer particles, creates the large scale structure of the polymer chain. The small number of polymer particles results in a decreased likelihood of an overlap between any of the polymer particles and the fluid molecules. Creating new polymer configurations by moving a large segment of primary particles increases the probability of large-scale polymer fluctuations, thus overcoming the slow sampling of the configuration space that plagues the traditional SMC. The averages over secondary chains inserted between adjacent primary polymer particles can then be used to calculate the statistical weight for the primary chain configuration.

The use of PIMC also allows the calculation of microscopic structural quantities which is not possible through DFT approximations. These can be used to ascertain the differences in polymer and fluid properties between localized and extended states. The polymer-fluid radial distribution function is important in computing the pickoff decay rate of orthopositronium in fluids. The results of calculations of structural quantities computed for Ps in xenon at 300 and 340 K indicate that, as the critical density is approached, the polymer particles are pushed closer together and the density of fluid molecules near the polymer center becomes markedly reduced. The decrease in fluid density indicates that a cavity is formed, while the decrease in polymer density at large distances from the polymer center indicates that the polymer particles become confined to the cavity. Comparisons between structural quantities calculated at $T=300$ and 340 K indicate that localization is slightly stronger at 300 than at 340 K. These results indicate that localization occurs more readily near the liquid-vapor critical point. Thus, the PIMC model has recreated an important result that is known from experimental measurements.

One of the major goals of this work was to determine if the PIMC technique could recreate the transition region of the experimental measurements of Ps annihilation in fluids. DFT approximations indicate that the LP is either trapped or extended, resulting in an unnatural discontinuity in decay rate predictions. In the PIMC technique, the transition is softened and compares more favorably with experiment.

It is interesting that R_T for the δ-function approximation was much closer to R_E than for the extended approximation. This may result from the Coulombic repulsion of the positron from the atomic nucleus, and suggests that the internal states of either or both the fluid atoms and positronium are altered by their mutual proximity. However, at the critical density, the theoretical calculations for the δ-function approximation did not deviate as much from the linear extrapolation as the experimental measurements. In our opinion, this constitutes a limitation of the present model. The fact that a flat "plateau" is found in experimental lifetime measurements in argon, xenon, and ethane, to name a few, led us to anticipate that this feature was robust, and would not be overly sensitive to the choice of potential. It was surprising that the semblance of a plateau could only be obtained from a very limited range of d. This suggests that, even in the critical region, the degree of localization depends sensitively on the details of the Ps-atom effective potential, and may partially explain the difficulties encountered by DFT in modeling the experimental data. It was recently pointed out to us that the hydrogen-atom–xenon potential may provide useful guidance for designing a more realistic Ps-Xe interaction potential [32].

A computation that takes into account all internal degrees of freedom would be unrealistic at this time. However, in future work it would be worthwhile to consider a model in which both the electron and positron in the Ps atom are represented by their own path integral. It would also be interesting to include the effect of polarization which, for xenon, could be considerable.

An intriguing feature of these calculations is the large variability in the Ps environment found at all densities. It strongly suggests that experimentalists should consider studying the distribution of annihilation rates in addition to extracting mean values from the data [33]. Some time ago McNutt and Sharma introduced a semiempirical

technique for computing the decay rate of orthopositronium which includes the effects of fluctuations at low and moderate densities [34]. A further use of the techniques developed here would be a microscopic *ab initio* test of their model.

ACKNOWLEDGMENTS

Computations were carried out using the CRAY Y computers at the Pittsburgh Supercomputing Center and the National Center for Supercomputing Applications. The authors benefited from conversations with D. Schrader, G. Worrell, D. Coker, and C. Morgenstern and are grateful for the support of the Robert Welch Foundation of Houston, Texas through Grant No. P-1002 and the Research Foundation of Texas Christian University. B.M. also benefited from the hospitality of the Theoretical Physics Department at the University of New South Wales during a visit.

[1] N. Gee and G. R. Freeman, Can. J. Chem. **64**, 1810 (1986).
[2] E. M. Juengerman, R. H. Argenbright, M. H. Ward, and S. C. Sharma, J. Phys. B **20**, 867 (1987).
[3] S. C. Sharma, R. H. Argenbright, and M. H. Ward, J. Phys. B **20**, 879 (1987).
[4] I. T. Iakubov and A. G. Khrapak, Prog. Phys. **45**, 697 (1982).
[5] B. N. Miller and T. L. Reese, Phys. Rev. A **39**, 4735 (1989).
[6] M. J. Stott and E. Zaremba, Phys. Rev. Lett. **38**, 1493 (1977).
[7] T. L. Reese and B. N. Miller, Phys. Rev. A **42**, 6068 (1990).
[8] B. N. Miller and Y. Fan, Phys. Rev. A **42**, 2228 (1990).
[9] M. Tuomisaari and K. Rytsola, in *Proceedings of the International Symposium on Positron Annihilation Studies of Fluids,* edited by S. C. Sharma (World Scientific, Singapore, 1989), p. 77.
[10] M. Tuomisaari, K. Rytsola, R. M. Nieminen, and P. Hautojarvi, J. Phys. B **19**, 2667 (1986).
[11] S. C. Sharma has carried out *o*-Ps lifetime measurements in ethane over an extended range of densities and temperatures (unpublished).
[12] L. D. Fosdick and H. F. Jordan, Phys. Rev. **143**, 58 (1966).
[13] D. Chandler and P. G. Wolynes, J. Chem. Phys. **74**, 4078 (1981).
[14] B. J. Berne and D. Thirumali, Ann. Rev. Phys. **37**, 401 (1986).
[15] R. P. Feynman and A. R. Hibbs, *Quantum Mechanics and Path Integrals* (McGraw-Hill, New York, 1965).
[16] A. L. Nichols III, D. Chandler, Y. Singh, and D. M. Richardson, J. Chem. Phys. **81**, 5109 (1984).
[17] N. Metropolis, A. W. Rosenbluth, M. N. Rosenbluth, A. H. Teller, and E. Teller, J. Chem. Phys. **21**, 1087 (1953).
[18] M. Sprik, M. L. Klein, and D. Chandler, Phys. Rev. B **31**, 4234 (1985); **32**, 545 (1984).
[19] R. A. Kuharski and P. J. Rossky, Chem. Phys. Lett. **103**, 35 (1984).
[20] M. Parrinello and A. Rahman, J. Chem. Phys. **80**, 860 (1984).
[21] D. F. Coker, B. J. Berne, and D. Thirumalai, J. Chem. Phys. **86**, 5689 (1987).
[22] J. Bartholomew, R. Hall, and B. J. Berne, Phys. Rev. B **32**, 548 (1985).
[23] G. Jacucci and E. Omerti, J. Chem. Phys. **79**, 3051 (1983).
[24] E. L. Pollock and D. M. Ceperley, Phys. Rev. B **30**, 2555 (1984); D. M. Ceperley and E. L. Pollock, Phys. Rev. Lett. **56**, 351 (1986).
[25] J. D. Doll and D. L. Freeman, J. Chem. Phys. **80**, 2239 (1984).
[26] G. A. Worrel and B. N. Miller, Phys. Rev. A **46**, 3380 (1992).
[27] J. A. Barker, J. Chem. Phys. **70**, 2914 (1979).
[28] P. A. Whitlock and M. H. Kalos, J. Comput. Phys. **30**, 361 (1978).
[29] Z. Liu and J. Broughton, Phys. Rev. B **40**, 571 (1989).
[30] The table of Hartree-Fock electron densities was provided by D. Schrader.
[31] P. Levy, *Memor. Sci. Math. Fasc. 126* (Gauthier-Villas, Paris, 1954).
[32] J. P. Toennies, W. Welz, and G. Wolf, J. Chem. Phys. **71**, 614 (1979).
[33] D. M. Schrader and S. G. Usmar, in *Proceedings of the International Symposium on Positron Annihilation Studies of Fluids* (Ref. [9]), Vol. 253.
[34] J. D. McNutt and S. C. Sharma, J. Chem. Phys. **68**, 130 (1978).